Multi-Satellite Retrieval of SSA using OMI-MODIS algorithm

Kruthika Eswaran[1,2*], Sreedharan Krishnakumari Satheesh[1, 2] and Jayaraman Srinivasan[1, 2]

[1] Centre for Atmospheric and Oceanic Sciences, Indian Institute of Science, Bangalore, India

[2] Divecha Centre for Climate Change, Indian Institute of Science, Bangalore, India

**Correspondence to:* Kruthika Eswaran (kruthika.eswaran89@gmail.com)

Abstract - Single scattering albedo (SSA) represents a unique identification of aerosol type and aerosol radiative forcing. However, SSA retrievals are highly uncertain due to cloud contamination and aerosol composition. The recent improvement in the SSA retrieval algorithm has combined the superior cloud-masking technique of the Moderate Resolution Imaging Spectroradiometer (MODIS) and the better sensitivity of the Ozone Monitoring Instrument (OMI) to aerosol absorption. The combined OMI-MODIS algorithm has been validated over a small spatial and temporal scale only. The present study validates the algorithm over global oceans for the period 2008-2012. The geographical heterogeneity in the aerosol type and concentration over the Atlantic Ocean, the Arabian Sea and the Bay of Bengal was useful to delineate the effect of aerosol type on the retrieval algorithm. We also noted that OMI overestimated SSA when absorbing aerosols were present closer to the surface. We attribute this overestimation to data discontinuity in the aerosol height climatology derived from Cloud-Aerosol Lidar and Infrared Pathfinder Satellite Observations (CALIPSO) satellite. OMI uses pre-defined aerosol heights over regions where CALIPSO climatology is not present leading to overestimation of SSA. The importance of aerosol height was also studied using the Santa Barbara DISORT radiative transfer (SBDART) model. The results from the joint retrieval were validated with ground-based measurements and it was seen that OMI-MODIS SSA retrievals performed better than OMI only retrieval over the Bay of Bengal during winter when the

aerosols are present closer to the surface. Discrepancy between satellite retrievals and cruise measurements was seen when elevated aerosols are present which might not be detected by the cruise instruments.

1. Introduction

Aerosols of different types are spatially distributed heterogeneously and at different altitudes in the atmosphere. Depending upon their properties, certain aerosols (biomass and carbon) warm the atmosphere by absorbing radiation, while other aerosols (sea salts and sulphates) cool the atmosphere by scattering radiation (Ramanathan et al., 2001). Due to the opposing effects on the atmosphere aerosols can have either net warming or cooling effect on the global climate depending upon the aerosol type, concentration and vertical distribution. Effect of natural and anthropogenic aerosols on the global climate is measured by 'aerosol radiative forcing' (the perturbation to the earth's radiation budget caused by the presence of aerosols). Positive forcing implies atmospheric warming and vice-versa. (Liao and Seinfeld, 1998; Podgorny and Ramanathan, 2001; Satheesh, 2002; Johnson et al., 2003; Kim et al., 2004; Moorthy et al., 2004; Meloni et al., 2005; Satheesh and Moorthy, 2005; Seinfeld and Pandis, 2006; Satheesh et al., 2008; Chand et al., 2009; Mishra et al., 2015). According to the climate assessment report, the estimation of aerosol radiative forcing (due to anthropogenic aerosols) is a major cause of uncertainty in the estimation of climate sensitivity and therefore presents a significant impediment to climate modelling (IPCC, 2013). The uncertainty is mostly due to the lack of accurate measurement of the scattering and absorbing properties of the aerosols (Cooke and Wilson, 1996; Menon et al., 2002; Chung and Seinfeld, 2002; Bond and Sun, 2005).

The Single Scattering Albedo (SSA), (the fraction of the total extinction of radiation attributed to scattering) is used to distinguish the scattering and absorbing properties of aerosols.

SSA represents a unique fingerprint of the type of aerosol and its radiative forcing (Hansen et al., 1997; Haywood et al., 1997; Myhre et al., 1998). In general, purely scattering aerosols have SSA value of approximately 1 while highly absorbing aerosols have SSA less than 0.7. However, SSA retrievals lack high certainty (Bond and Bergstrom, 2006; Bond et al., 2013). Uncertainties in SSA retrievals are due to factors such as cloud contamination, instrumentation error and aerosol modification due to atmospheric processes. A small change in SSA can cause the aerosol radiative forcing to change from negative to positive (Hansen et al., 1997; Seinfeld and Pandis, 2006). Loeb and Su (2010) performed a radiative perturbation analysis and found that direct aerosol radiative forcing was highly sensitive to small perturbations in SSA under clear-sky and cloudy-sky conditions. A simulation study using Santa Barbara DISORT Radiative Transfer (SBDART) model in the present work (Section 5.3) shows that a change in SSA from 0.8 to 1 can induce a change of 4 Wm^{-2} in the top-of-atmosphere (TOA) flux depending on the aerosol type and aerosol layer height (Figure 8). Better SSA retrievals (both in-situ and satellite-based) are required to reduce the uncertainty in SSA for a more accurate estimation of aerosol forcing; particularly over regions influenced by a variety of air masses. There is also a need for accurate spectral aerosol absorption measurements, which is required to validate SSA derived from satellites (Bergstrom et al., 2007).

Studies on the various measurements of aerosol light absorption using instruments and their uncertainty evaluation have been performed previously (Horvath, 1993, Heintzenberg et al., 1997; Moosmuller et al., 2009). The different methods of retrieval of SSA, both ground-based and using satellites, are provided in Table 1. Unlike aerosol absorption coefficient, SSA is not measured directly by an instrument. Instead, it is retrieved using lookup tables or estimated using other parameters which are measured or calculated using models.

Though these previous studies on ground-based retrievals have brought a fundamental understanding to the estimation of amounts of aerosols / aerosol chemistry, their restricted spatial and temporal extent is a significant limitation. Moreover, these studies have reduced availability of scenes for indirect retrievals. Some techniques are limited due to cloud contamination while others operate only under specific conditions (e.g. presence of sun glint). This presents a need for better SSA retrieval algorithms that overcome the present technical limitations and that can be applied on a global scale. The global extent of observations from satellites has increased the spatial extent of the observations (Kaufman et al., 2002a). Though the satellite-based SSA retrievals have been shown to be extremely successful over the majority of ocean and land regions, they still have a limited success over deserts and ice sheets. Over deserts and ice-sheets, high surface reflectance affects the satellite retrievals in the visible spectrum. To counter this, SSA is retrieved in the UV spectrum (330 nm to 400 nm) over these regions (Torres et al., 1998, 2007). In the UV spectrum, the upwelling radiances are highly sensitive to the aerosol absorption and also have a lower influence of surface albedo (Torres et al., 2007). SSA retrieval in UV spectrum hence avoids difficulties encountered over surfaces with high albedo.

The quality of OMI SSA retrievals is affected by sub-pixel cloud contamination (due to the larger footprint of size 13km x 24km) and the spectral surface albedo (Torres et al., 2007). To counter the problems and uncertainties in the OMI SSA retrieval (Table 2), Satheesh et al. 2009 used retrievals from multiple satellites. They used combined retrievals from OMI-MODIS since each of these sensors have their own strengths and both fly within ~7-8 minutes of each other in the A-train constellation (Stephens et al., 2002). The better cloud-screened retrieval of AOD from MODIS (Levy et al., 2003) and the high sensitivity of OMI to aerosol absorption was used to develop a hybrid algorithm to retrieve SSA (Satheesh et al., 2009). The algorithm uses the

MODIS AOD as a reference to infer the aerosol layer height and SSA from OMI. This removes any *a priori* assumption made by the OMI algorithm regarding an aerosol model. The study by Satheesh et al. 2009 was performed over the East tropical Atlantic Ocean, the Central tropical Atlantic Ocean and the Arabian Sea for the year 2006. A comparison of the retrieved aerosol height with aircraft measurements showed that OMI-MODIS was more accurate than OMI. Gassó and Torres (2016) performed a detailed analysis of the OMI UV product retrievals over oceans and island sites. They compared the OMI retrieved AOD with MODIS and AERONET (Aerosol Robotic Network) AODs. They also used the OMI-MODIS algorithm for only two particular cases over and near Africa to understand how the assumption of aerosol height and shape affected AOD and SSA retrievals. It was found that when the actual height from satellite Lidar was used instead of climatological values and when the shape of dust aerosols was assumed to be non-spherical, the retrievals by OMI agreed better with other observations including the original OMI-MODIS method. The OMI-MODIS algorithm has been used in calculating aerosol radiative forcing (Satheesh et al., 2010) over oceanic regions surrounding India and used in retrieving SSA over land (Narasimhan and Satheesh, 2013) as well as used to understand the retrievals of OMI UV products for two particular cases (Gassó and Torres, 2016). However, a detailed analysis of the algorithm on a larger spatial and temporal scale has not been done so far.

The current work applies the OMI-MODIS algorithm to retrieve SSA on a global scale. It is applied over the global oceans from 2008-2012. Regional analysis over the Atlantic, the Arabian Sea and the Bay of Bengal are done by incorporating the aerosol layer height and the type of aerosols. After estimating SSA values using the OMI-MODIS algorithm, the present study then uses cruise measurements of SSA from the Integrated Campaign for Aerosols, Gases and

Radiation Budget (ICARB) and winter ICARB campaigns over Arabian Sea and Bay of Bengal in 2006 and 2009 to validate the same (Moorthy et al., 2008, 2010).

2. Data

2.1. OMI

The Ozone Monitoring Instrument (OMI) onboard the Aura satellite was launched in 2004. For OMI measurements two aerosol inversion schemes are used- OMI near UV (OMAERUV) algorithm and the multi-wavelength (OMAERO) algorithm (Torres et al., 2007). The OMAERO algorithm uses 19 wavelengths in the range of 330-500 nm to retrieve corresponding aerosol characteristics. For the present study, we have used the OMAERUV algorithm which uses measurements at two wavelengths 354 nm and 388 nm. The reason behind choosing these wavelengths is the high sensitivity of upwelling radiances to aerosol absorption and the lower influence of surface in measurements due to low reflectance values in the UV region. In addition to this, the wavelengths also have negligible interference from trace gases. This gives a unique advantage of retrieving aerosol properties over ocean and land including arid and semi-arid regions (Torres et al., 1998; 2007).

The products derived from the algorithm include AOD, absorption aerosol optical depth (AAOD) and single scattering albedo (SSA). These are derived from pre-computed reflectance values for different aerosol models. Three major types of aerosols have been used - Desert dust, carbonaceous aerosols from biomass burning and background and urban-industrial aerosols. Each type has seven models of SSA. The retrieved products of OMAERUV are sensitive to the aerosol layer height (Torres et al., 1998) and are reported for five discrete aerosol layer heights, i.e., surface (exponential profile), 1.5, 3.0, 6.0, and 10.0 km with latter four following a Gaussian distribution.

Due to the high sensitivity of SSA retrieval to the assumption of aerosol height and aerosol type (Torres et al., 2002), the OMI algorithm was improved (Collection 003-PGE V1.4.2, Torres et al., 2013). The climatology of aerosol layer height from CALIPSO (Cloud-Aerosol Lidar and Infrared Pathfinder Satellite Observations) along with carbon monoxide (CO) measurements from AIRS (Atmospheric Infrared Sounder) have helped distinguish carbonaceous aerosols from dust particles. Torres et al. (2013) showed that the combined use of AIRS CO measurements and OMI Aerosol Index (AI) retrievals, helped in identifying the type of absorbing aerosol. Thus, smoke layers were identified when values of AI and CO measurements were high and during events of high AI and low CO values, the aerosols were identified as dust. The AIRS CO measurements were also used to identify large aerosol loading which was otherwise represented as clouds by the OMAERUV algorithm. Using collocated observations of OMI and Cloud-Aerosol Lidar with Orthogonal Polarization (CALIOP), Torres et al. (2013) estimated the height of elevated absorbing aerosols for a 30-month period from July 2006 to December 2008. An effective aerosol layer height was calculated using the CALIOP 1064 nm attenuated backscatter weighted by corresponding altitudes. The 30-month climatology of aerosol height was used in the OMAERUV retrievals which then validated against the AERONET observations (Torres et al., 2013). The results showed that there was an improvement in the retrievals.

Since 2007, observations have been affected by an instrumental issue called the *row anomaly* which reduces the quality of radiance at all wavelengths (Jethva et al., 2014). Torres et al. (2018) studied the impact of row anomaly on the OMAERUV retrievals by comparing monthly values AOD, SSA and UV aerosol index (UVAI) of two different sets of scattering angles. Over regions dominated by carbonaceous and sulphate aerosols, the agreement between the sets was better than over arid regions dominated by dust aerosols. Differences were also

found over cloudy regions. The discrepancies were attributed to the inaccurate representation of scattering effects of dust aerosols and cloud droplets. Better representation of scattering by clouds and the non-spherical (spheroidal) shape assumption of dust aerosols was found to reduce the inconsistencies in aerosol products due to row anomaly. These improvements have been incorporated in the latest version of OMAERUV product (version 1.8.9) which has been used in the present study. Along with the aerosol products retrieved at different heights, the final set of AOD/SSA/AAOD retrievals in the OMAERUV product is reported at the mean ALH provided by the 30-month long averaged climatology developed using OMI-CALIOP combined observations (Torres et al., 2013). The original aerosol height assumptions were used in the algorithm over regions where the climatology was unavailable.

2.2. MODIS

The Moderate Resolution Imaging Spectrometer (MODIS) instrument on the Aqua satellite was launched in 2002. This instrument, with 36 spectral channels has a unique ability to retrieve aerosol properties with better accuracy over both land and ocean (Remer et al., 2005; Levy et al., 2003). Of these, seven channels (0.47-2.13 μm) are used to retrieve aerosol properties over the ocean (Tanré et al., 1997).

As described in Remer et al., (2005), before the retrieval algorithm, masking of sediments, clouds and ocean glint is performed to separate valid pixels from bad ones. The retrieval algorithm of MODIS (also called the inversion procedure) has been described in detail previously (Tanré et al., 1997; Levy et al., 2003; Remer et al., 2005). The algorithm uses a 'look-up table' (LUT) approach, i.e., for a set of aerosol and surface parameters, radiative transfer calculations are performed. Spectral reflectance derived from the LUT is compared with MODIS-measured spectral reflectance to find the 'best' (least-squares) fit. The resulting

combination of modes provides the aerosol model from which size distribution, properties including spectral optical depth, effective radius etc. are derived. The product used from MODIS is the Level 2 aerosol (MYD04, Collection 5.1) product. The parameter chosen is 'Effective_Optical_Depth_Average_Ocean' which provides the aerosol optical depth over the ocean at seven wavelengths. The value is the average of all the solutions in the inversion procedure with the least-square error < 3%.

A combination of OMI and MODIS helps indirectly in counteracting the cloud contamination problem and also uses the strength of the individual sensors – OMI's sensitivity to aerosol absorption combined with the better cloud screening of MODIS and accurate retrieval of AOD, and aerosol size (Satheesh et al., 2009; Narasimhan and Satheesh, 2013).

3. Algorithm

MODIS aerosol product reports retrievals at 10 x 10 km spatial resolution at nadir (and a cloud mask at 500m and 1km resolution) whereas OMI reports at 13 km x 24 km. This results in an OMI pixel being prone to cloud contamination which may result in an overestimation in AOD and SSA (Torres et al., 1998). However, AAOD can be retrieved in the presence of small cloud contamination since there is cancellation of errors (Torres et al., 2007).

The high accuracy of size-resolved aerosol retrievals with MODIS is because the over-ocean algorithm employs all seven channels (0.47-2.13 micron) in the inversion enabling better characterization of fine and coarse particles. (Tanré et al., 1997; Remer et al., 2005; Levy et al., 2003). While OMI is highly sensitive to aerosol absorption in the near-UV region, the accuracy in the retrieval of AAOD depends on the aerosol layer height assumption. OMI provides AOD and AAOD at different heights as prescribed by various aerosol types (Torres et al., 2007).

The assumption of aerosol layer height in the OMI algorithm constraints the retrievals of

AOD and SSA. The approach proposed in Satheesh et al. (2009) used MODIS AOD as an input to the OMI retrieval algorithm, so that the MODIS AOD constraints the OMI inversion so that the OMI inversion is free to infer the aerosol layer height and SSA. Satheesh et al. (2009) extrapolated MODIS AOD from the visible to 388nm and compared the estimated UV AOD with high quality ground-based AERONET observations. The deviation between linearly-extrapolated MODIS AOD and AERONET AOD was more significant at higher AERONET AOD values. This was attributed to the presence of a large number of fine-mode aerosols which caused a nonlinear curvature to the AOD spectral dependence and affected AOD at UV wavelengths. Hence to improve the linear extrapolation, information on the aerosol spectral curvature was also included. This was achieved by using an average regression equation to correct the MODIS AOD (Satheesh et al., 2009; Equation 3). They showed that MODIS AOD could be first linearly extrapolated to 388 nm and then corrected for curvature before being used as input to the OMI retrieval algorithm. The present work uses the same algorithm as proposed by Satheesh et al. (2009) to retrieve SSA over the oceans for the region 60S-60N and 180W-180E from December 2007-November 2012. The methodology is described in detail in the following section.

4. Methodology

The AOD for ocean obtained from the Level 2 aerosol product of Aqua-MODIS (MYD04) was used. Using linear extrapolation with spectral curvature correction (Satheesh et al., 2009), AOD at 388 nm (hereafter, AOD_{388}) was calculated from AOD at seven wavelengths ranging from 0.47-2.13 μm. OMI provides AOD and SSA for five different aerosol layer heights starting from the surface and at 1.5, 3.0, 6.0 and 10.0km (AOD_{OMI} and SSA_{388}). It also provides the best estimate of SSA calculated based on the CALIOP aerosol layer height climatology (SSA_{OMI}).

For the present study, polar regions are not included and hence pixels from both OMI and

MODIS that are outside the 60S-60N and 180W-180E region are excluded. Pixels with invalid or missing values are also excluded. The various parameters extracted from the data were re-gridded onto a uniform grid of 0.5˚ x 0.5˚ within the region of study to reduce computation time. For both the satellites, this procedure was repeated for each swath data which were then combined to calculate the daily means.

The daily data from collocated MODIS and OMI were utilised in the final algorithm. As mentioned before OMI provides AOD and SSA for five different aerosol layer heights. Using AOD_{388} as the reference, the corresponding aerosol layer height was calculated from the five AOD_{OMI} values through linear interpolation. This height is then used as a reference to find the SSA using interpolation from the set of SSA_{388} values. Finally, this SSA ($SSA_{OMI\text{-}MODIS}$), and the best estimate of SSA (SSA_{OMI}) were compared with each other.

5. Results

The spatial distribution of SSA retrieved using OMI is shown in Fig. 1a. The values are averaged over five years and plotted seasonally.

The SSA retrieved using OMI-MODIS algorithm is shown in Fig. 1b.

SSA over open oceans is close to 1 due to the presence of a large amount of sea-salt and sulphate. Closer to land, a variety of aerosols are present which results in SSA varying from 0.85 to ~1. Over the oceans, separation of ocean colour effects and aerosol concentrations is difficult. Hence the OMI algorithm retrieves when enough absorbing aerosols are present, i.e.AI >=0.8 (Torres et al., 2013). Only pixels whose quality has been assigned as 0 or the highest quality by OMI have been used. The points flagged for row anomaly are also not used in this study. Thus, the retrievals did not cover the entire globe. From Fig.1a it can be seen that majority of the valid SSA retrievals were over major aerosol sources in the world and not over remote oceanic regions

like central equatorial Pacific or Antarctic ocean. The major sources include the vast biomass outflow over the Atlantic Ocean from the west coast of Africa, the dust over the Arabian Sea from the arid areas of Arabia & Africa and the dust blown over the Atlantic Ocean from the Sahara. Other regions like the east coast of China, the Bay of Bengal are influenced by a variety of anthropogenic aerosols during different seasons. In the OMI-MODIS algorithm, the aerosol layer height is retrieved through linear interpolation of AOD_{OMI} at five different heights and AOD_{388} as a reference. Linear interpolation was not performed for OMI retrievals which had a missing value at any particular height or if the OMI retrieval was the same at all heights. Such OMI-MODIS values were considered to be invalid. Similarly, if the MODIS AOD was found to be missing or invalid, the corresponding OMI-MODIS retrieval was also considered invalid. This resulted in a reduction in the total number of valid points in OMI-MODIS algorithm when compared to OMI algorithm (Fig. 1b). However, both the algorithms capture the major oceanic regions which are influenced by a large number of aerosols. Gassó and Torres (2016) for a particular day over the North Central Atlantic compared the AOD values retrieved by OMI and MODIS. They compared the difference with the aerosol cloud mask retrieved by MODIS. It was found that while most of the retrievals of OMI screened the cloudy pixels, some of the best quality (flag=0) pixels were found to be cloud contaminated. This they attributed to the coarser pixel size of OMI compared to the smaller pixel size of MODIS cloud product. At higher cloud fraction, OMI retrieved values implying that they can detect aerosol above clouds or the pixels are prone to cloud contamination. Gassó and Torres concluded that only MODIS cloud fraction could not be used to screen out OMI pixels. A larger spatiotemporal scale of such an analysis is required but is beyond the scope of this manuscript and will be addressed in the future. However, OMI retrievals at higher cloud fraction could be the reason for more points in Fig. 1a than OMI

MODIS in Fig. 1b.

Two important regions over oceans influenced by a variety of aerosols are the tropical Atlantic Ocean and the oceans around the Indian subcontinent. The new approach was used over these regions- Atlantic (5N-30N; 60W-20W) (ATL) and Arabian Sea and Bay of Bengal (0-25N; 55E-100E) (ARBOB).

5.1. Difference in SSA retrieval algorithms during different seasons

To understand how the OMI-MODIS algorithm compares with the retrieval using the existing OMI algorithm, the difference between $SSA_{OMI\text{-}MODIS}$ and SSA_{OMI} (ΔSSA) averaged over five years for different seasons is shown in Fig. 2.

During March-April May (MAM) and June-July-August (JJA), there is a longitudinal gradient in ΔSSA from the coast of Sahara towards the open Atlantic Ocean. Kaufman et al. (2002a) showed that close to the coast of Africa, aerosols are more absorbing than those away from the coast. The difference in the type of aerosols as we move away from the coast could be one of the reasons for the gradient in ΔSSA. The difference can also be attributed to the shape of dust aerosols which are present in large numbers near the coast of Africa (Torres et al., 2018). The ΔSSA changes sign with season. This was attributed to the change in aerosol layer height and (or) aerosol physical and optical properties.

Both ATL and ARBOB regions are influenced by the type of aerosols which result in a complex mixture and eventually resulting in the variation in SSA distribution over each season. While the spatial plot of ΔSSA in Fig. 2 represents the regions where maximum and minimum differences are located around the globe, a distribution plot provides the ranges of ΔSSA which dominate and which do not. The distribution of ΔSSA for different seasons averaged over five years (2008-2012) is plotted in Fig. 3a and 3b for the regions- ATL and ARBOB respectively.

Over the tropical Atlantic Ocean, ΔSSA was found within ±0.03 >80% of the time during all the seasons. Over Arabian Sea and Bay of Bengal, the values of SSA matched within ±0.03 during MAM when dust is present in large quantity over the region. However, ΔSSA has values lower than <-0.03 especially during the seasons of JJA and SON. Satheesh et al. (2009) showed in their analysis that the reason for the discrepancies during non-dust seasons could be due to the wrong assumption of aerosol layer height (ALH) or due to the wrong assumption of aerosol model. Before understanding the role of ALH in SSA retrieval, the meteorological conditions of the ARBOB region (Arabian Sea and Bay of Bengal separately), for different seasons are studied and trajectory analysis is done. This helps in identifying major sources of aerosols during each season.

5.2. Trajectory analysis

Arabian Sea and Bay of Bengal (ARBOB)

The Arabian Sea and the Bay of Bengal are oceanic regions on the west and east coast of India respectively. Both regions are influenced by various types of aerosols during different seasons. The Arabian Sea has been dominated by dust aerosols and is influenced by high levels of dust during certain seasons as seen from satellite images (Sirocko and Sarnthein, 1989). Pease et al. (1998) studied the geochemistry and the transport of various dust samples during different cruises in different seasons. During winter and summer, the pattern of aerosol transport was similar to that of the Indian monsoon pattern – northeasterly (winter) and southwesterly (summer). Thus, the major sources of aerosols were the Arabian Peninsula (including Saharan dust and the Middle East) and Indian sub-continent in summer and winter respectively. The mean 7-day back trajectory using HYSPLIT model from a point over the Arabian Sea (15N; 65E) was performed for each season of 2010 and at three different heights (500m, 1500m and 2500m

above MSL). The Arabian Sea region was divided into four quadrants – 1) Arabian Peninsula and North Africa, 2) Central Africa, 3) Indian sub-continent and 4) Indian Ocean and Southeast Asia (Fig. 4). The influence of different aerosol source regions over the Arabian Sea is given in Table 2.

Similar to Pease et al. (1998), Tindale and Pease (1999) found that transport of aerosols near the surface followed the surface wind currents. The dust content was low near the surface during summer due to the presence of Findlater jet, but the general dust concentrations were higher than other oceanic regions. During winter, the winds are predominantly north and northeasterly and hence results in transport of aerosols from India/Pakistan/Afghanistan onto the Arabian Sea. However, the presence of anticyclonic circulation over Arabia (20N; 60E) results in northwesterly winds transporting dust over the Arabian Sea (Rajeev et al., 2000). The springtime (March-April-May) is the transition between northeast and southwest monsoon. The winds become south westerlies which result in the advection of aerosols from the open Indian Ocean or near Somalia. At higher altitudes (above the Findlater jet) dust transport occurs from Arabia. During summer, the southwest monsoon wind patterns carry aerosols all the way from southeast/east Indian Ocean (mainly sea-salt). As the altitude increases, the wind patterns change a little due to aerosols coming from southwest Indian Ocean/Somalia. Above the Findlater jet, as explained by Tindale and Pease (1999), dust transport occurs from Arabian Peninsula (Table 2).

Being an integral part in the Indian Summer Monsoon, studies over the Bay of Bengal is important especially the role of aerosols in the local climate change. While the Arabian Sea is dominated by dust and oceanic aerosols, studies have shown that the Bay of Bengal is influenced by various air masses associated with Asian monsoon system including those of anthropogenic origin (Krishnamurti et al., 1998). The synoptic meteorological conditions over the Bay of

Bengal have been studied in detail by Moorthy et al. (2003) and Satheesh et al. (2006). Similar to the other two regions, mean 7-day back trajectory analysis from a point over (15N; 90N) was performed for each season of 2010 and at three different heights (500m, 1500m and 2500m above MSL). The four quadrants representing the various aerosol source regions are 1) India/Arabian Peninsula, 2) Indian Ocean, 3) North/Northeast India and East Asia and 4) Southeast Asia (Fig. 5). Table 3 represents the influence of aerosol source regions over the Bay of Bengal.

The northwesterly winds occur from west to east in the Indo-Gangetic Plain (IGP) and due to subsidence, the aerosols are trapped in the east during winter (Dey and Di Girolamo, 2010; Di Girolamo et al., 2004). The IGP with its heavy population and large number of industries acts as a source for anthropogenic aerosols which are transported to Bay of Bengal during winter (Kumar et al., 2013). Along with mineral dust from the Arabian Peninsula, biomass aerosols from Southeast Asia are also transported to the bay. Field experiments like ICARB (Moorthy et al., 2008) during the springtime (pre-monsoon) showed transports of aerosols from the Arabian Peninsula and also the presence of elevated aerosols (anthropogenic and natural) over Bay of Bengal (Satheesh et al., 2008). The post-monsoon season acts as a transition from the summer to winter monsoon. The winds during September are still south westerlies and during October weak westerlies are present (Lawrence and Lelieveld, 2010). This results in transportation of aerosols from the Indian Ocean and the Arabian Sea. Thus, from Table 3 it can be seen that both anthropogenic aerosols (from IGP, Southeast Asia) and natural aerosols (marine and dust) are present over the Bay of Bengal during different seasons.

5.3. Role of Aerosol Layer Height in SSA retrieval

Satheesh et al. (2009) devised a new algorithm to improve the retrieval of SSA using

combined OMI and MODIS data. They used MODIS-predicted UV AOD as the input to improve the original OMI algorithm, which was constrained by the assumption of aerosol layer height. Over the Atlantic, they found that on an average the AOD values retrieved from both algorithms agreed within ±0.1. However, over the Arabian Sea only when there was considerable loading of dust (especially during the March-April-May season), the OMI AOD and MODIS AOD had agreement suggesting that during other seasons, the assumption of aerosol height could be wrong. Satheesh et al. (2009) also found that over the Arabian Sea the aerosol layer height (ALH) derived from OMI-MODIS algorithm agreed well with aircraft measurements when compared to OMI SSA retrieval. In the current work, the aerosol layer height (ALH) provide by OMI, is the mean climatological height (section 2.1). For OMI-MODIS the ALH is estimated from OMI AOD values (at five different heights) by linear interpolation using AOD_{388} as a reference (section 4). The difference in aerosol layer height (ALH) between OMI-MODIS and OMI was plotted against the difference in SSA over the Arabian Sea and Bay of Bengal (Fig. 6a). The colorbar represents ALH estimated by OMI-MODIS algorithm. The most important observation from this analysis was that OMI overestimated SSA when it overestimated ALH (compared to OMI-MODIS) and vice versa. It has been shown by Gassó and Torres (2016) that when the actual aerosol height measured by Satellite Lidar was 1.5km more than the climatological or assumed height, OMI retrieved higher SSA. It can be seen from Fig. 6a, the blue coloured circles represent height estimated by OMI-MODIS between the surface to ~ 2km. In this range, it was seen that the height assumed by OMI is > 1.5km compared to the one estimated by OMI-MODIS. Thus, OMI overestimated SSA compared to the OMI-MODIS retrieval.

Gassó and Torres (2016), in their detailed analysis of the OMI UV aerosol product (version

1.4.2), studied the OMI-MODIS method for two specific cases. They have mentioned that when the extrapolated MODIS 388nm AOD was not within the OMI LUT values, the OMI-MODIS algorithm retrieves unrealistic height and SSA. For the ARBOB region, the difference in AOD ($AOD_{MODIS} - AOD_{OMI}$) has been plotted with the difference in SSA ($SSA_{OMI\text{-}MODIS} - SSA_{OMI}$) (Fig. 6b). The colorbar represents the difference in ALH ($ALH_{OMI\text{-}MODIS} - ALH_{OMI}$) retrieved by both the algorithms. An inverse relation was seen implying that when OMI underestimated AOD compared to MODIS, OMI overestimated SSA compared to OMI-MODIS. The difference in AOD was mainly within the ±0.5 range. However, there are a few points where the AOD difference was >3. Mostly in such cases, the difference between the ALH and SSA estimates of both the algorithms was high. However, there are points when the AOD difference was high and the ALH and SSA differences were within ±1 km and ±0.03 respectively. Similarly, the difference between ALH and SSA values of both the algorithms was high when the AOD difference was within ±0.5. These discrepancies could be attributed to the AOD spectral curvature of an aerosol type assumed by MODIS which is different by the aerosol model assumed by OMI UV aerosol product (Gassó and Torres, 2016). Whether any other property apart from AOD and shape (for dust aerosols) can affect the ALH and SSA retrievals have to be studied in the future.

The importance of ALH and SSA in the calculation of TOA flux was studied using the Santa Barbara DISORT (SBDART) model (Ricchiazzi et al., 1998). For the same tropical environment variables and surface albedo of 0.06, the SSA was varied from 0.8 to 1 and aerosol height from 0 to 10 km at 1 km interval. The simulations were done for a narrow band in UV (300-400nm). For a constant AOD, AE (Angstrom Exponent) and asymmetry factor (0.4, 1 and 0.7 respectively), TOA flux was calculated (Fig. 7a). It can be seen that at any ALH, TOA flux varied with SSA.

The role of ALH is important in the UV region due to the phenomena of Rayleigh scattering (van de Hulst, 1981). The importance of Rayleigh scattering on the role of ALH is further shown in Fig. 7b. In this particular set of simulations, the Rayleigh scattering is completely removed and all other parameters are kept the same as in Fig. 7a. It can be seen that once molecular scattering is removed, the effect of ALH is also removed and TOA flux depends only on SSA and other aerosol properties. The basis of many aerosol retrievals by satellites in the UV spectrum is the sensitivity of aerosol absorption to Rayleigh scattering which acts as a bright background and contributes to the TOA radiance (Torres et al., 1998; 2002). Change in ALH can affect the TOA radiance since the aerosol layer will interact with the Rayleigh scattering due to molecules present in the atmosphere. However, this effect is smaller compared to the effect due to the change in AOD and SSA (Kim et al., 2018). Kim et al. (2018) also showed how the misclassification of aerosol type and size could affect ALH retrieval. OMI SSA retrievals which are based on LUT depend on the ALH assumed along with aerosol type. The SBDART simulations in the current work show how for a particular TOA flux, SSA varies with ALH when the other aerosol properties are kept constant.

5.4. Comparison between SSA retrievals from OMI and OMI-MODIS with ship-borne estimates.

To validate the new retrieval method of SSA using OMI and MODIS, both SSA values from OMI and OMI-MODIS were compared with ground-based measurements (SSA at 450nm) during cruises in the period 2006 and 2009 in the Arabian Sea and Bay of Bengal. These cruises were part of the Integrated Campaign for Aerosols, gases and Radiation Budget (ICARB) performed during the months of March to May 2006 and once during winter (W-ICARB) from 27 December 2008 to 30 January 2009 (Moorthy et al., 2008 and 2010). During both the cruises

438 the aerosol sampling was done onboard the Oceanic Research Vessel *Sagar Kanya*. While the
439 2006 cruise covered both the Arabian Sea and the Bay of Bengal, the winter cruise of 2009
440 covered the Bay of Bengal. The cruise tracks are provided in detail in Moorthy et al., 2008 and
441 2010, respectively. The SSA values at different wavelengths were estimated from spectral values
442 of the absorption coefficient and scattering coefficient measured using the instruments
443 Aethalometer (Magee Scientific AE-31, USA) and an integrating nephelometer (TSI 3563, USA)
444 respectively. More details about the instrument and measuring techniques including the
445 uncertainties are provided in Nair et al. (2008). However, both the cruise did not estimate SSA
446 values in the UV spectrum. The closest wavelength at which SSA is calculated is 450nm which
447 has been used to compare with the satellite retrievals of SSA (388nm). Ground-based SSA
448 estimates based on in-situ measurements are seldom consistent with columnar satellite retrievals
449 especially when elevated aerosols are present. This uncertainty along with the uncertainty in the
450 assumption of SSA being uniform between 388nm and 450nm implies that the current
451 comparison of study cannot be used as a validation study. Instead, it is used to understand the
452 consistency of SSA retrievals from satellites with ground-based observations. Since the cruise
453 measurements had little coverage spatially, for better coverage, a 2° box was used around each
454 location within which the mean SSA was calculated for the respective cruise period. These
455 values are plotted in Fig. 8. OMI comparison is given by circles and OMI-MODIS by square
456 markers. It can be seen that despite using a 2° box, the number of points having valid SSA values
457 for the cruise and the satellite retrievals was only 21. This number increased as the size of the
458 box around each cruise location was increased. The low number is due to the sparse nature of the
459 OMI-MODIS retrieval over the region (Fig. 1b). The colour scale represents the cruise and the
460 region where the aerosol sampling was taken.

During the ICARB, presence of elevated aerosols at a height of ~1km-3km have been shown in earlier studies (Satheesh et al., 2008; Nair et al., 2009). In such cases comparison between a ship-based aerosol retrieval which detects aerosols close to the surface and the SSA retrieval from satellites which detects these elevated aerosols cannot be considered appropriate. This discrepancy was seen in Fig. 8 especially over the Arabian Sea (Blue colour) and some points over Bay of Bengal (Red). In some cases, OMI was able to retrieve SSA consistent with the cruise estimated, unlike OMI-MODIS. This could be due to the improvement of dust model assumption in the new version of OMI aerosol product and (or) due to the wrong spectral AOD dependence assumed by MODIS. During the winter most of the aerosols influencing the Bay of Bengal is present closer to the surface. In such cases comparing the SSA estimates can be valid. It was observed that during winter when aerosols are generally present close to the surface, OMI-MODIS retrieved SSA which is a bit more consistent with the ship estimates compared to OMI. In such cases, OMI still overestimated SSA despite the improvement in the algorithm. The respective RMSEs for OMI and OMI-MODIS comparison with the cruise estimates were 0.05 and 0.06. Due to the lack of common points, the correlation was also poor (OMI-MODIS: 0.11 and OMI: -0.35).

The OMI-MODIS approach in SSA retrieval is one of the many combinations of sensors that can be used in retrieving aerosol properties. A better approach involving the vertical distribution of aerosols either from space or ground-based observations is required to reduce the uncertainty further. However, with few ground-based measurements in the UV regime especially over the oceans and fewer retrievals of the vertical aerosol absorption, validation of new algorithms is still in the nascent stage.

6. Summary and Conclusions

Aerosol forcing depends on aerosol properties like aerosol optical depth (AOD) and single scattering albedo (SSA). SSA is highly sensitive to the aerosol composition and size and as well as the wavelength at which the aerosol interacts with radiation. A slight change in SSA value can alter the sign of the forcing. Hence it is important to have an accurate measurement of SSA globally. The Ozone Monitoring Instrument (OMI) retrieves SSA in the UV spectrum. However, these retrievals are affected by cloud contamination and are sensitive to aerosol layer height. In addition to these problems, uncertainty in the surface albedo is a source of error for SSA retrieval. To resolve the issue of sub-pixel cloud contamination, Satheesh et al. (2009) developed a method using the combination of OMI and the Moderate Resolution Imaging Spectroradiometer (MODIS) at a local scale. In the present study, we used the method developed by Satheesh et al. (2009) to retrieve SSA at a much larger spatial and temporal scale. The main findings from our study are listed below:

1. Both OMI and OMI-MODIS algorithms retrieved SSA over regions influenced by large amounts of aerosols (e.g. Atlantic Ocean – ATL; Arabian Sea and Bay of Bengal – ARBOB)
2. The difference in SSA retrievals of both the algorithms (ΔSSA) was found to be within ±0.03 over ATL >80% of the time during all the seasons. Over the Arabian Sea, as seen in Satheesh et al. (2009), ΔSSA was within the ±0.03 range during MAM when the region was influenced by dust. The discrepancy during other season was due to the wrong assumption of aerosol layer height by OMI.
3. From Fig. 6a it was seen that OMI overestimated SSA when it overestimated ALH and vice versa. This could be attributed to the wrong assumption of aerosol height. Fig. 6b

showed that difference in AOD and difference in SSA had an inverse relationship. Further analysis on whether any other factor apart from ALH and aerosol shape can affect SSA retrieval has to be studied.

4. Both SSA retrievals were compared with cruise data from the ICARB and W-ICARB campaigns in the Arabian Sea and Bay of Bengal.
5. While both the algorithms did not match the cruise estimate during most of the dust season due to the presence of elevated aerosols, in few cases during ICARB, OMI performed better than OMI-MODIS. This could be due to the better assumption of dust model in the algorithm and/or wrong model assumption by MODIS. During winter, when the aerosols were present closer to the surface, OMI-MODIS was a bit more consistent compared to OMI. This may be due to scenarios where the CALIPSO climatology was absent and OMI used its previous aerosol model assumptions. This could also be due to uncertainties in ALH value even after the improvement in the OMI algorithm with the addition of CALIPSO climatology.

OMI retrieves aerosol properties at high cloud fraction (Gassó and Torres, 2016) implying two things, either OMI is able to detect aerosols present above clouds or the OMI pixel was prone to cloud contamination. In their study, Gassó and Torres (2016), observed that while MODIS cloud fraction could be used to screen out cloudy pixels in OMI, it could not be the lone criterion. While they performed for a single case, an analysis of a larger spatial and temporal scale is required. Aerosol type and aerosol layer height play a vital role in the retrieval of aerosol properties. Without the assumption of aerosol type or height, OMI-MODIS provided SSA retrievals which was consistent with cruise estimates during the winter when the Bay of Bengal was influenced by anthropogenic aerosols present close to the surface. This was not the case

when dust aerosols were present. This discrepancy can be attributed to the difference in the aerosol model assumption by MODIS and OMI. This comparison study had very few points for a detailed analysis. Hence, an accurate comparison and validation of such retrieval algorithms can be possible only when there are more ground-based observations available in the UV spectrum on a larger spatial and temporal scale along with vertical profiles of aerosol absorption.

Acknowledgements

The authors gratefully acknowledge the NOAA Air Resources Laboratory (ARL) for the provision of the HYSPLIT transport and dispersion model used in this publication. The authors are grateful to NASA data and services centre.

References

Bergstrom, R.W., Pilewskie, P., Russell, P.B., Redemann, J., Bond, T.C., Quinn, P.K., and Sierau, B.: Spectral absorption properties of atmospheric aerosols, Atmos. Chem. Phys., 7, 5937-5943, 2007.

Bond, T.C., and Sun, H.: Can reducing black carbon emissions counteract global warming?, Environ. Sci. Technol., 39(16), 5921-5926, 2005.

Bond, T.C., and Bergstrom, R.W.: Light absorption by carbonaceous particles: An investigative review, Aerosol Sci. Tech., 40(1), 27-67, doi:10.1080/02786820500421521, 2006.

Bond, T.C., Doherty, S.J., Fahey, D.W., Forster, P.M., Bernsten, T., De Angelo, B.J., Flanner, M.G., Ghan, S., Karcher, B., Koch, D., Kinne, S., Kondo, Y., Quinn, P.K., Sarofim, M.C., Schultz, M., Venkataraman, C., Zhang, H., Zhang, S., Bellouin, N., Guttikunda, S.K., Hopke, P.K., Jacobson, M.Z., Kaiser, J.W., Klimont, Z., Lohmann, U., Schwarz, J.P., Shindell, D., Storelvmo, T., Warren, S.G., and Zender, C.S.: Bounding the role of black carbon in the climate system: A scientific assessment, J. Geophys. Res., 118(11), 5380-

553 5552, doi:10.1002/jgrd.50171, 2013.
554 Chand, D., Wood, R., Anderson, T.L., Satheesh, S.K., and Charlson, R.J.: Satellite-derived direct
555 radiative effect of aerosols dependent on cloud cover, Nat. Geosci., 2, 181–184,
556 doi:10.1038/ngeo437, 2009.
557 Chung, S.H., and Seinfeld, J.H.: Global distribution and climate forcing of carbonaceous
558 aerosols, J. Geophys. Res., 107(D19), 4407, doi:10.1029/2001JD001397, 2002.
559 Cooke, W.F., and Wilson, J.J.N.: A global black carbon aerosol model, J. Geophys. Res., 101,
560 19395-19410, doi:10.1029/96JD00671, 1996.
561 Dey, S., and Di Girolamo, L.: A climatology of aerosol optical and microphysical properties over
562 the Indian subcontinent from 9 years (2000–2008) of Multiangle Imaging
563 Spectroradiometer (MISR) data, J. Geophys. Res., 115, D15204,
564 doi:10.1029/2009JD013395, 2010.
565 Di Girolamo, L., Bond, T.C., Bramer, D., Diner, D.J., Fettinger, F., Kahn, R.A., Mrtonchik, J.V.,
566 Ramana, M.V., Ramanathan, V., and Rasch, P.J.: Analysis of Multi-angle Imaging
567 SpectroRadiometer (MISR) aerosol optical depths over greater India during winter 2001-
568 2004, Geophys. Res. Lett., 31(23), L23115, doi:10.1029/2004GL021273, 2004.
569 Diner, D.J., Beckert, J.C., Reilly, T.H., Bruegge, C.J., Conel, J.E., Kahn, R.A., Martonchik, J.V.,
570 Ackerman, T.P., Davies, R., Gerstl, S.A.W., Gordon, H.R., Muller, J.-P., Myneni, R.B.,
571 Sellers, P.J., Pinty, B., and Verstraete, M.M.: Multi-angle Imaging SpectroRadiometer
572 (MISR) instrument description and experiment overview, IEEE T GEOSCI REMOTE,
573 36(4), 1072-1087, doi:10.1109/36.700992, 1998.
574 Dubovik, O., and King, M.D.: A flexible inversion algorithm for retrieval of aerosol optical
575 properties from Sun and sky radiance measurements, J. Geophys. Res., 105(D16), 20673-

20696, doi:10.1029/2000JD900282, 2000.

Dubovik, O., Holben, B.N., Eck, F.T., Smirnov, A., Kaufman, Y.J., King, M.D., Tanré, D., and Slutsker, I.: Variability of absorption and optical properties of key aerosol types observed in worldwide locations, J. Atmos. Sci., 59(3), 590-608, doi:10.1175/1520-0469(2002)059<0590:VOAAOP>2.0.CO;2, 2002.

Eck, T.F., Holben, B.N., Slutsker, I., and Setzer, A.: Measurements of irradiance attenuation and estimation of aerosol single scattering albedo for biomass burning aerosols in Amazonia, J. Geophys. Res., 103(D24), 31865-31878, doi:10.1029/98JD00399, 1998.

Gassó, S., and Torres, O.: The role of cloud contamination, aerosol layer height and aerosol model in the assessment of the OMI near-UV retrievals over the ocean, Atmos. Meas. Tech., 9, 3031-3052, doi:10.5194/amt-9-3031-2016, 2016.

Hansen, J., Sato, M., and Ruedy, R.: Radiative forcing and climate response, J. Geophys. Res.-Atmos., 102(D6), 6831-6864, doi:10.1029/96JD03436, 1997.

Harriss, R.C., Browell, E.V., Sebacher, D.I., Gregory, G.L., Hinton, R.R., Beck, S.M., McDougal, D.S., and Shipley, S.T.: Atmospheric transport of pollutants from North America to the North Atlantic Ocean, Nature, 308, 722-724, doi:10.1038/308722a0, 1984.

Haywood, J.M., Roberts, D.L., Slingo, A., Edwards, J.M., and Shine, K.P.: General circulation model calculations of the direct radiative forcing by anthropogenic sulphate and fossil-fuel soot aerosol, J. Clim., 10, 1562-1577, doi:10.1175/1520-0442(1997)010<1562:GCMCOT>2.0.CO;2, 1997.

Heintzenberg, J., Charlson, R.J., Clarke, A. D., Liousse, C., Ramaswamy, V., Shine, K.P., Wendish, M., and Helas, G.: Measurements and modelling of aerosol single-scattering albedo: Progress, problems and prospects, Contrib. Atmos. Phys., 70(4), 249– 263, 1997.

599 Herman, B.M., Browning, R.S., and De Luisi, J.J.: Determination of the effective imaginary term
600 of the complex refractive index of atmospheric dust by remote sensing: the diffuse-direct
601 radiation method, J. Atmos. Sci., 32, 918-925, doi:10.1175/1520-
602 0469(1975)032<0918:DOTEIT>2.0.CO;2, 1975.
603 Herman, J.R., Bhartia, P.K., Torres, O., Hsu, C., Seftor, C., and Celarier, E.: Global distribution
604 of UV-absorbing aerosols from Nimbus 7/TOMS data, J. Geophys. Res.-Atmos., 102(D14),
605 16911-16922, doi:10.1029/96JD03680, 1997.
606 Horvath, H.: Atmospheric light absorption- a review, Atmos. Environ. A-Gen., 27(3), 293-317,
607 doi:10.1016/0960-1686(93)90104-7, 1993.
608 Intergovernmental Panel on Climate Change (IPCC) (2013), The physical science basis:
609 Contribution of Working Group I to the Fifth Assessment Report of the Intergovernmental
610 Panel on Climate Change, In: Climate Change (2013), Stocker, T.F., D. Qin, G.K. Plattner,
611 M. Tignor, S.K. Allen, J. Boschung, A. Nauels, Y. Xia, V. Bex, and P.M. Midgley (eds),
612 Cambridge University, Press: Cambridge, United Kingdom and New York, NY, USA 1535
613 pp, doi:10.1017/CBO9781107415324.
614 Jethva, H., Torres O., and Ahn C.: Global assessment of OMI aerosol single-scattering albedo
615 using ground-based AERONET inversion, J. Geophys. Res.-Atmos., 119(14), 9020-9040,
616 doi:10.1002/2014JD021672, 2014.
617 Johnson, B.T., Shine, K.P., and Forster, P.M.: The semi-direct aerosol effect: Impact of absorbing
618 aerosols on marine stratocumulus, Q. J. Roy. Meteor. Soc., 130, 1407-1422,
619 doi:10.1256/qj.03.61, 2003.
620 Kaufman, Y.J.: Satellite sensing of aerosol absorption, J. Geophys. Res., 92, 4307-4317,
621 doi:10.1029/JD092iD04p04307, 1987.

622 Kaufman, Y.J., Tanré, D., and Boucher, O.: A satellite view of aerosols in the climate system,
623 Nature, 419, 215-223, doi:10.1038/nature01091, 2002a.
624 Kaufman, Y.J., Martins, J.V., Remer, L.A., Schoeberl, M.R., and Yamasoe, M.A.: Satellite
625 retrieval of aerosol absorption over the oceans using sunglint, Geophys. Res. Lett., 29(19),
626 34-1 – 34-4, doi:10.1029/2002GL015403, 2002b.
627 Kaufman, Y.J., Koren, I., Remer, L.A., Tanré, D., Ginoux, P., and Fan, S.: Dust transport and
628 deposition observed from the Terra-Moderate Resolution Imaging Spectroradiometer
629 (MODIS) spacecraft over the Atlantic Ocean, J. Geophys. Res., 110, D10S12,
630 doi:10.1029/2003JD004436, 2005.
631 Kim, S-W., Yoon, S-C., Jefferson, A., Won, J-G., Dutton, E.G., Ogren, J.A., and Anderson T.L.:
632 Observation of enhanced water vapour in Asian dust layer and its effect on atmospheric
633 radiative heating rates, Geophys. Res. Lett., 31(18), doi:10.1029/2004GL020024, 2004.
634 Kim, M., Kim, J., Torres, O., Ahn, C., Kim, W., Jeong, U., Go, S., Liu X., Moon, K.J., and Kim,
635 D.-R.: Optimal Estimation-Based Algorithm to Retrieve Aerosol Optical Properties for
636 GEMS Measurements over Asia, Remote Sens., 10(2), 162, doi:10.3390/rs10020162, 2018.
637 King, M.D.: Determination of the ground albedo and the index of absorption of atmospheric
638 particulates by remote sensing. Part II: Application, J. Atmos. Sci., 36, 1072-1083,
639 doi:10.1175/1520-0469(1979)036<1072:DOTGAA>2.0.CO;2, 1979.
640 Krishnamurti, T.N., Jha, B., Prospero J., Jayaraman, A., and Ramanathan, V.: Aerosol and
641 pollutant transport and their impact on radiative forcing over the tropical Indian Ocean
642 during the January – February 1996 pre-INDOEX cruise, Tellus B, 50(5): 521–542,
643 doi:10.1034/j.1600-0889.1998.00009.x, 1998.
644 Kumar, K.R., Sivakumar, Reddy, R.R., and Gopal, K.R.: Ship-borne measurements of columnar

and surface aerosol loading over the Bay of Bengal during W-ICARB campaign: role of airmass transport. Latitudinal and Longitudinal Gradients, Aerosol Air Qual Res., 13, 818–837, doi:10.4209/aaqr.2012.08.0225, 2013.

Lawrence, M.G., and Lelieveld, J.: Atmospheric pollutant outflow from southern Asia: a review, Atmospheric Chemistry and Physics, 10, 11017-11096, doi:10.5194/acp-10-11017-2010, 2010.

Levy, R.C., Remer, L.A., Tanré, D., Kaufman, Y.J., Ichoku, C., Holben, B.N., Livingston, J.M., Russell, P.B., and Maring, H.: Evaluation of the Moderate-Resolution Imaging Spectroradiometer (MODIS) retrievals of dust aerosol over the ocean during PRIDE, J. Geophys. Res., 108(D19), 8594, doi:10.1029/2002JD002460, 2003.

Liao, H., and Seinfeld, J.H.: Radiative forcing by mineral dust aerosols: Sensitivity to key variables, J. Geophys. Res.-Atmos., 103(D24), 31637-31645, doi:10.1029/1998JD200036, 1998.

Meloni, D., di Sarra, A., di Lorio, T., and Fiocco, G.: Influence of the vertical profile of Saharan dust on the visible direct radiative forcing, J. Quant. Spectrosc. Ra., 93(4), 397-413, doi:10.1016/j.jqsrt.2004.08.035, 2005.

Menon, S., Hansen, J., Nazarenko, L., and Luo, Y.: Climate effects of black carbon aerosols in China and India, Science, 297(5590), 2250-2253, doi:10.1126/science.1075159, 2002.

Mishra, A.K., Koren, I., and Rudich, Y.: Effect of aerosol vertical distribution on aerosol-radiation interaction: A theoretical prospect, Heliyon, e00036, doi:10.1016/j.heliyon.2015.e00036, 2015.

Moorthy, K.K., Babu, S.S., and Satheesh, S.K.: Aerosol spectral optical depths over the Bay of Bengal: role of transport, Geophys. Res. Lett., 30(5): 1249, doi:10.1029/2002GL016520,

2003.

Moorthy, K.K., Babu, S.S., Sunilkumar, S.V., Gupta, P.K., and Gera, B.S.: Altitude profiles of aerosol BC, derived from aircraft measurements over an inland urban location in India, Geophys. Res. Lett., 31(22), 10.1029/2004GL021336, 2004.

Moorthy, K.K., Satheesh, S.K., Babu, S.S., and Dutt, C.B.S.: Integrated campaign for aerosols, gases and radiation budget (ICARB): an overview, J. Earth. Syst. Sci., 117(1), 243-262, doi:10.1007/s12040-008-0029-7, 2008.

Moorthy, K.K., Beegum, S.N., Babu, S.S., Smirnov, A., John, S.R., Kumar, K.R., Narasimhulu, K., Dutt, C.B.S., and Nair, V.S.: Optical and physical characteristics of Bay of Bengal aerosols during W-ICARB: spatial and vertical heterogeneities in the marine atmospheric boundary layer and in the vertical column, J. Geophys. Res., 115(D24): D24213, doi:10.1029/2010JD014094, 2010.

Moosmuller, H., Chakrabarty, R.K., and Arnott, W.P.: Aerosol light absorption and its measurement: A review, J. Quant. Spectrosc. Ra., 110(11), 844-878, doi:10.1016/j.jqsrt.2009.02.035, 2009.

Morris, V., Colon, P.C., Nalli, N.R., Joseph, E., Armstrong, R.A., Detres, Y., Goldberg, M.D., Minnett, P.J., and Lumpkin, R.: Measuring Trans-Atlantic aerosol transport from Africa, EOS Trans. AGU, 87(50), 565-571, doi:10.1029/2006EO500001, 2006.

Myhre, G., Stordal, F., Restad, K., and Isaksen, I.S.A.: Estimation of the direct radiative forcing due to sulphate and soot aerosols, Tellus, 50B, 463-477, 1998.

Nair, V.S., Babu, S.S., and Moorthy, K.K.: Spatial distribution and spectral characteristics of aerosol single scattering albedo over the Bay of Bengal inferred from shipborne measurements, Geophys. Res. Lett., 35, doi:10.1029/2008GL033687, 2008.

691 Nair V.S., Moorthy, K.K., and Babu, S.S.: Optical and Physical Properties of Atmospheric
692 Aerosols over the Bay of Bengal during ICARB, J. Atmos. Sci., 66, doi:
693 10.1175/2009JAS3032.1, 2009.
694 Narasimhan, D., and Satheesh, S.K.: Estimates of aerosol absorption over India using multi-
695 satellite retrieval, Ann. Geophys., 31, 1773-1778, doi:10.5194/angeo-31-1773-2013, 2013.
696 Pease, P.P., Tchakerian, V.P., and Tindale, N.W.: Aerosols over the Arabian Sea: geochemistry
697 and source areas for Aeolian desert dust, J. Arid Environ., 39(3), 477-496,
698 doi:10.1006/jare.1997.0368, 1998.
699 Podgorny, I.A., and Ramanathan, V.: A modeling study of the direct effect of aerosols over the
700 tropical Indian Ocean, J. Geophys. Res., 106(D20): 24097–24105,
701 doi:10.1029/2001JD900214, 2001.
702 Prospero, J.M., and Carlson, T.N.: Vertical and areal distribution of Saharan dust over the
703 western equatorial north Atlantic Ocean, J. Geophys. Res., 77(27), 5255-5265,
704 doi:10.1029/JC077i027p05255, 1972.
705 Prospero, J.M.: Saharan dust transport over the North Atlantic Ocean and Mediterranean: An
706 overview, In: The Impact of Desert Dust Across the Mediterranean, Guerzoni S., Chester
707 R. (Eds.), 133-151, doi:10.1007/978-94-017-3354-0_13, 1996.
708 Rajeev, K., Ramanathan, V., and Meywerk, J.: Regional aerosol distribution and its long-range
709 transport over the Indian Ocean, J. Geophys. Res.-Atmos., 105(D2), 2029-2043,
710 doi:10.1029/1999JD900414, 2000.
711 Ramanathan, V., Crutzen, P.J., Kiehl, J.T., and Rosenfield, D.: Aerosols, climate and the
712 hydrological cycle, Science, 294(5549): 2119–2124, doi:10.1126/science.1064034, 2001.
713 Remer, L. A., Kaufman, Y. J., Tanré, D., Mattoo, S., Chu, D. A., Martins, J. V., Li, R. R., Ichoku,

C., Levy, R. C., Kleidman, R. G., Eck, T. F., Vermote, E., and Holben, B. N.: The MODIS aerosol algorithm, products, and validation, J. Atmos. Sci., 62, 947–973, doi:10.1175/JAS3385.1, 2005.

Ricchiazzi, P., Yang, S., Gautier, C., and Sowle, D.: SBDART: a research and teaching software tool for plane-parallel radiative transfer in the earth's atmosphere, B. Am. Meteorol. Soc. 79(10): 2101–2114, doi:10.1175/1520-0477(1998)079<2101: SARATS>2.0.CO;2, 1998.

Satheesh, S.K.: Aerosols and climate, Resonance, 7(4), 48-59, doi:10.1007/BF02836138, 2002.

Satheesh, S.K., and Moorthy, K.K.: Radiative effects of natural aerosols: a review, Atmos. Environ., 39(11): 2089–2110, doi:10.1016/j.atmosenv.2004.12.029, 2005.

Satheesh, S.K., Srinivasan, J., and Moorthy, K.K.: Spatial and temporal heterogeneity in aerosol properties and radiative forcing over Bay of Bengal: Sources and role of aerosol transport, J. Geophys. Res., 111(D8): D08202, doi:10.1029/2005JD006374, 2006.

Satheesh, S.K., Moorthy, K.K., Babu, S.S., Vinoj, V., and Dutt, C.B.S.: Climate implications of large warming by elevated aerosol over India, Geophys. Res. Lett., 35(19), doi:10.1029/2008GL034944, 2008.

Satheesh, S.K., Torres, O., Remer, L.A., Babu, S.S., Vinoj, V., Eck, T.F., Kleidman, R.G., and Holben, B.N.: Improved assessment of aerosol absorption using OMI-MODIS joint retrieval, J. Geophys. Res., 114, D05209, doi:10.1029/2008JD011024, 2009.

Satheesh, S.K., Vinoj, V., and Moorthy, K.K.: Assessment of aerosol radiative impact over oceanic regions adjacent to Indian subcontinent using multi-satellite analysis, Adv. Meteorol., 2010, Article ID 139186, pp 13., doi:10.1155/2010/139186, 2010.

Seinfeld, J.H., and Pandis, S.N.: Atmospheric Chemistry and Physics: From air pollution to climate change, 2nd Ed., 1232 pp, John Wiley & Sons, Inc., Hobkoben, New Jersey, 2006.

737 Sirocko, F., and Sarnthein, M.: Wind-borne deposits in the northwestern Indian Ocean: Record of
738 Holocene sediments versus modern satellite data, In: Paleoclimatology and
739 Paleometeorology: modern and past patterns of global atmospheric transport, Leinen M.,
740 Sarnthein M. (Eds), 401-433, Amsterdam: Kluwer Academic Publishers, 1989.
741 Stephens, G.L., Vane, D.G., Boain, R.J., Mace, G.G., Sassen, K., Wang, Z., Illingworth, A.J.,
742 O'Connor, E.J., Rossow, W.B., Durden, S.L., Miller, S.D., Austin, R.T., Benedetti, A.,
743 Mitrescu, C., and CloudSat Science Team: The CloudSat mission and the A-Train: A new
744 dimension of space-based observations of clouds, precipitation, B. Am. Meteorol. Soc., 83,
745 1771-1790, doi:10.1175/BAMS-83-12-1771, 2002.
746 Tanré, D., Kaufman, Y.J., Herman, M., and Mattoo, S.: Remote sensing of aerosol properties
747 over oceans using the MODIS/EOS spectral radiances, J. Geophys. Res., 102(D14),
748 16971–16988, 1997.
749 Tindale, N.W., and Pease, P.P.: Aerosols over the Arabian Sea: Atmospheric transport pathways
750 and concentrations of dust and sea salt, Deep-Sea Res. Pt. II, 46(8-9), 1577-1595,
751 doi:10.1016/S0967-0645(99)00036-3, 1999.
752 Torres, O., Bhartia, P. K., Herman, J. R., and Ahmad, Z.: Derivation of aerosol properties from
753 satellite measurements of backscattered ultraviolet radiation. Theoretical Basis, J.
754 Geophys. Res., 103(D14), 17099–17110, 1998.
755 Torres, O., Decae, R., Veefkind, J.P., and de Leeuw, G.: OMI aerosol retrieval algorithm, in OMI
756 Algorithm Theoretical Basis Document: Clouds, Aerosols, and Surface UV Irradiance, 3,
757 V2, OMIATBD- 03, edited by P. Stammes, pp. 47 – 71, NASA Goddard Space Flight
758 Cent., Greenbelt, Md, 2002.
759 (http://eospso.gsfc.nasa.gov/eos_homepage/for_scientists/atbd/docs/OMI/ATBD-OMI-

760 03.pdf)
761 Torres, O., Bhartia, P.K., Sinyuk, A., Welton, E.J., and Holben, B.: Total Ozone Mapping
762 Spectrometer measurements of aerosol absorption from space: Comparison to SAFARI
763 2000 ground-based observations, J. Geophys. Res., 110(D10), doi:10.1029/2004JD004611,
764 2005.
765 Torres, O., Tanskanen, A., Veihelmann, B., Ahn, C., Braak, R., Bhartia, P.K., Veefkind, P., and
766 Levelt, P.: Aerosols and surface UV products from Ozone Monitoring Instrument
767 observations: An overview, J. Geophys. Res., 112, D24S47, doi:10.1029/2007JD008809,
768 2007.
769 Torres, O., Ahn, C., and Chen, Z.: Improvements to the OMI near-UV aerosol algorithm using A-
770 train CALIOP and AIRS observations, Atmos. Meas. Tech., 6, 3257-3270,
771 doi:10.5194/amt-6-3257-2013, 2013.
772 Torres, O., Bhartia, P.K., Jethva, H., and Ahn, C.: Impact of the ozone monitoring instrument row
773 anomaly on the long-term record of aerosol products, Atmos. Meas. Tech., 11, 2701-2715,
774 doi:10.5194/amt-11-2701-2018, 2018.
775 Van de Hulst, H.C.: Light scattering by small particles, 496 pp., Dover publications, New York,
776 1981.
777 Wells, K.C., Martins, J.V., Remer, L.A., Kreidenweis, S.M., and Stephens, G.L.: Critical
778 reflectance derived from MODIS: Application for the retrieval of aerosol absorption over
779 desert regions, J. Geophys. Res., 117(D3), doi:10.1029/2011JD016891, 2012.
780 Zhu, L., Martins, J.V., and Remer, L.A.: Biomass burning aerosol absorption measurements with
781 MODIS using the critical reflectance method, J. Geophys. Res., 116(D7),
782 doi:10.1029/2010JD015187, 2011.

783 Zuluaga, M.D., Webster, P.J., and Hoyos, C.D.: Variability of aerosols in the tropical Atlantic
784 Ocean relative to African Easterly Waves and their relationship with atmospheric and
785 oceanic environments, J. Geophys. Res., 117(D16), doi:10.1029/2011JD017181, 2012.

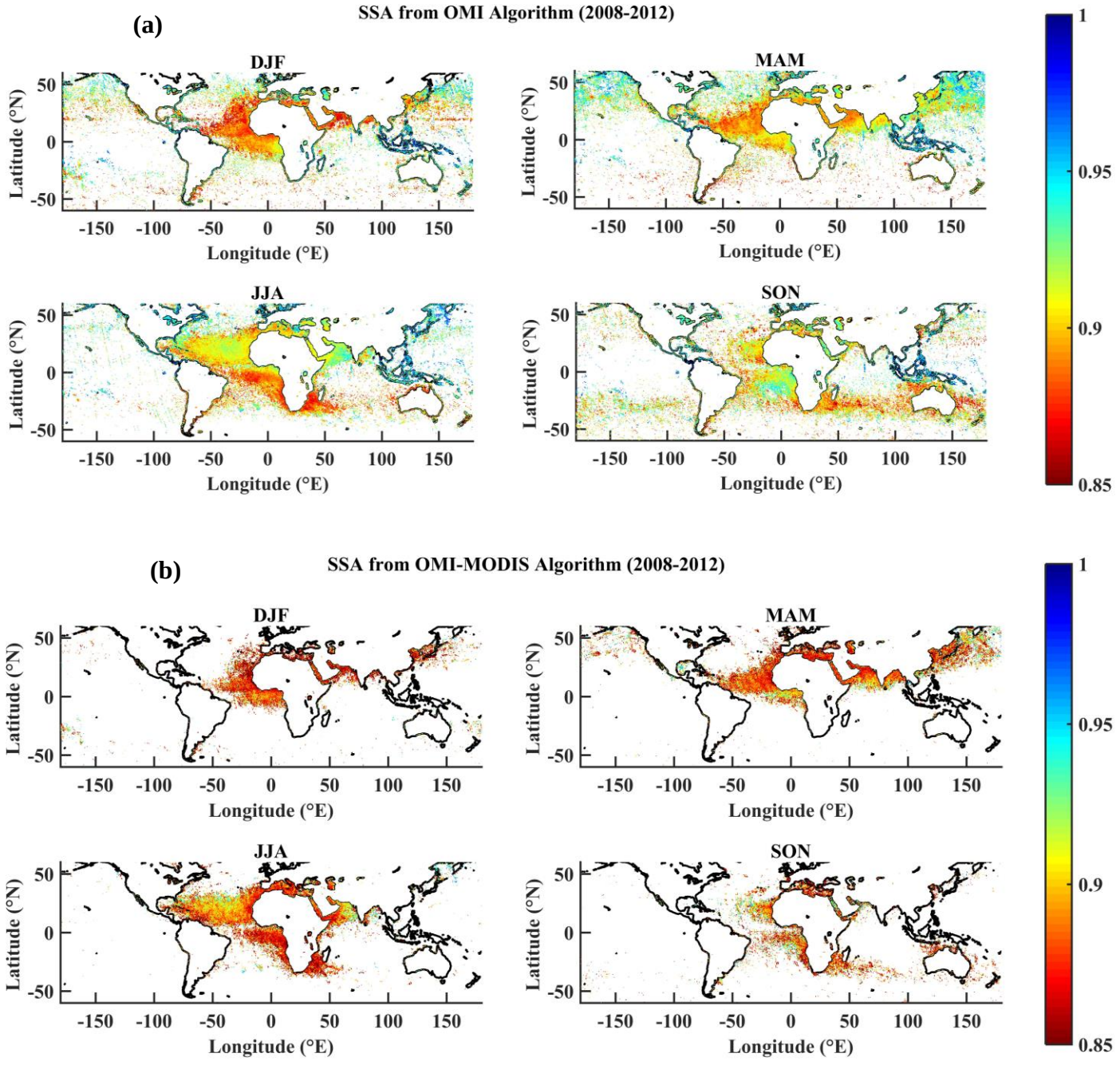

786

787

788 **Figure 1.** Spatial distribution of SSA at 388nm retrieved by a) OMI and b) OMI-MODIS. In the
789 present study, points which had the same SSA value at the 5 discrete heights provided by OMI or

790 an invalid value at any one height were considered invalid for the OMI-MODIS retrieval since
791 interpolation was not possible. This resulted in the reduction of the number of valid points for
792 OMI-MODIS when compared to OMI.

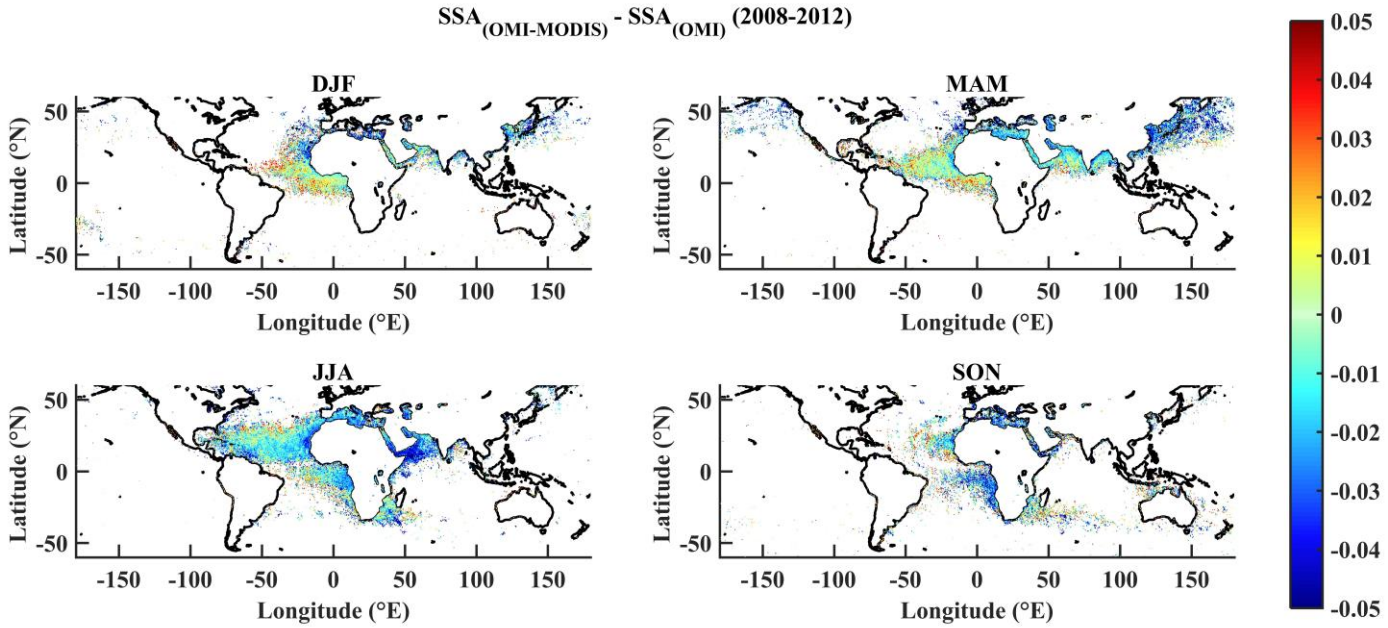

793

794 **Figure 2.** Spatial distribution of difference in SSA retrieved by OMI-MODIS and SSA retrieved
795 by OMI, both at 388nm. When the OMI-MODIS SSA value was found invalid, the difference
796 was also considered to be invalid.

797

798

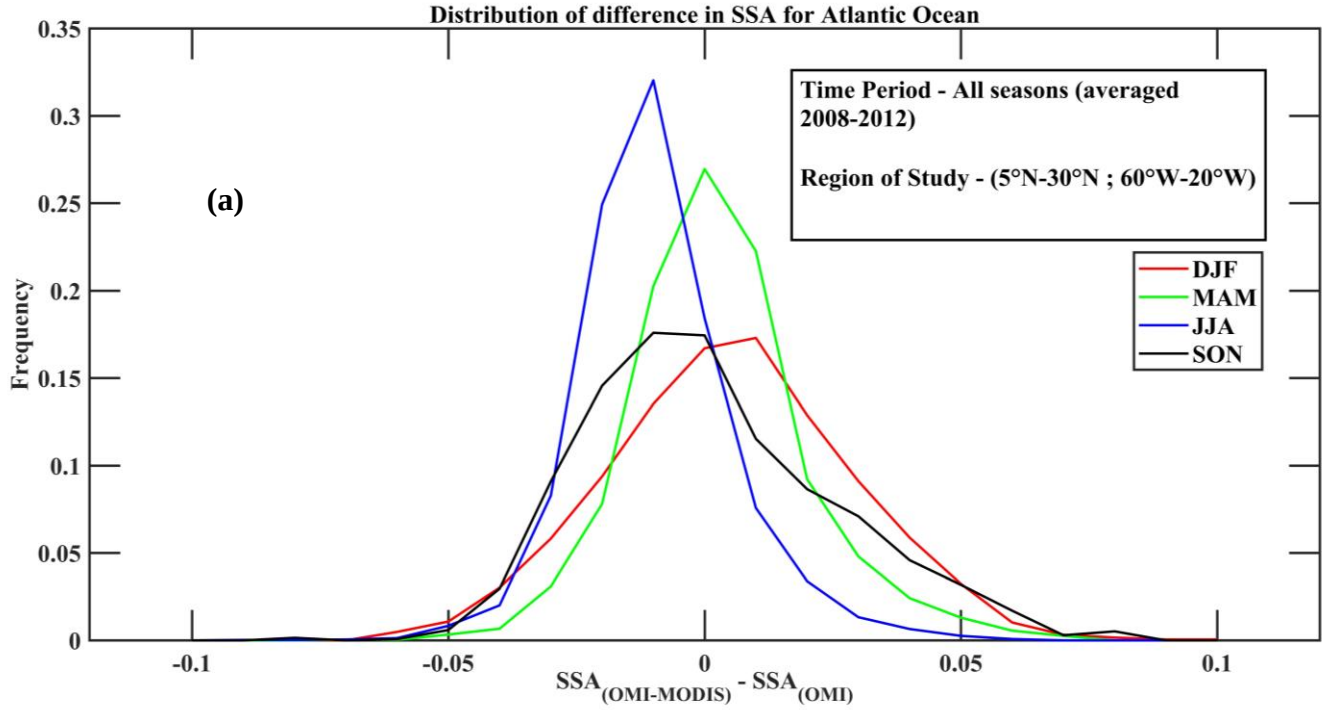

799

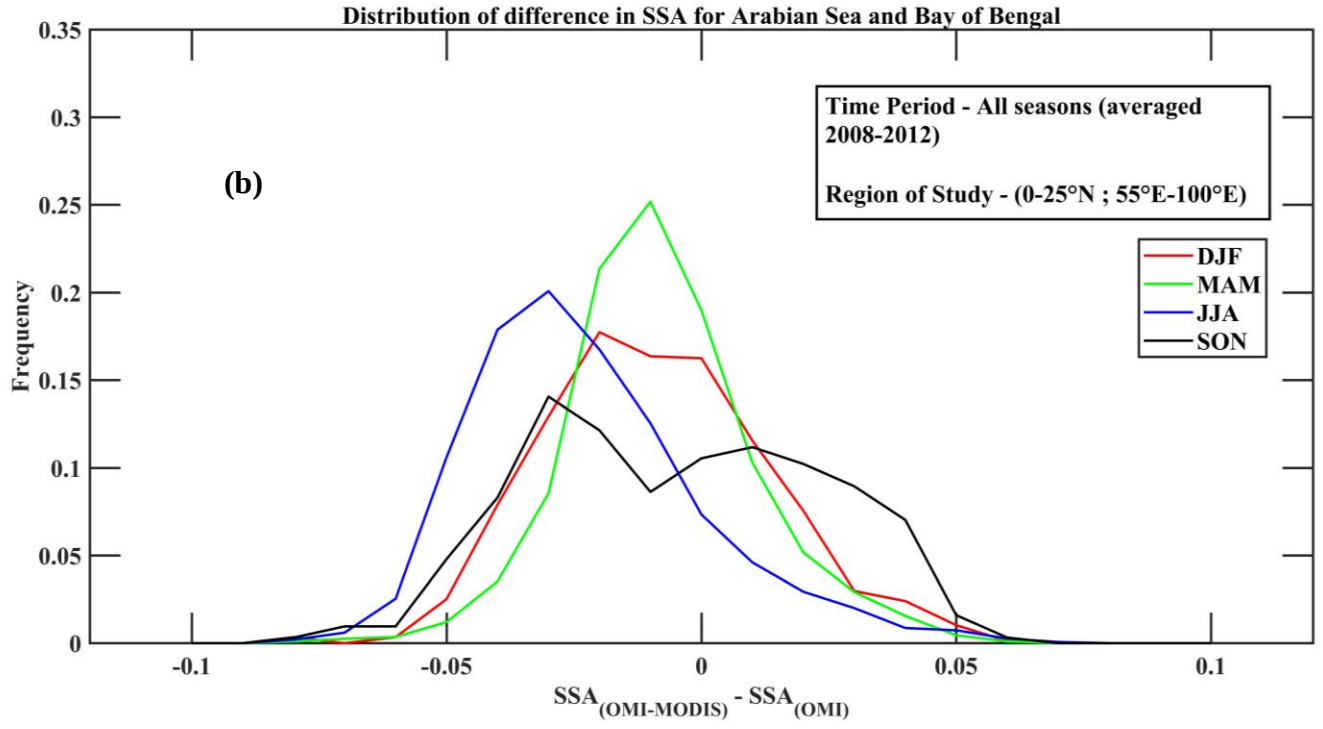

800

801 **Figure 3.** Distribution of difference in SSA for all seasons averaged over 2008-2012 over a)
802 Atlantic and b) Arabian Sea and Bay of Bengal. It can be seen that over the Atlantic Ocean, 80%

of the difference in SSA retrievals was within the ±0.03 range. Over the Arabian Sea and Bay of Bengal, the retrievals agreed well during the MAM season when the region was influenced by dust.

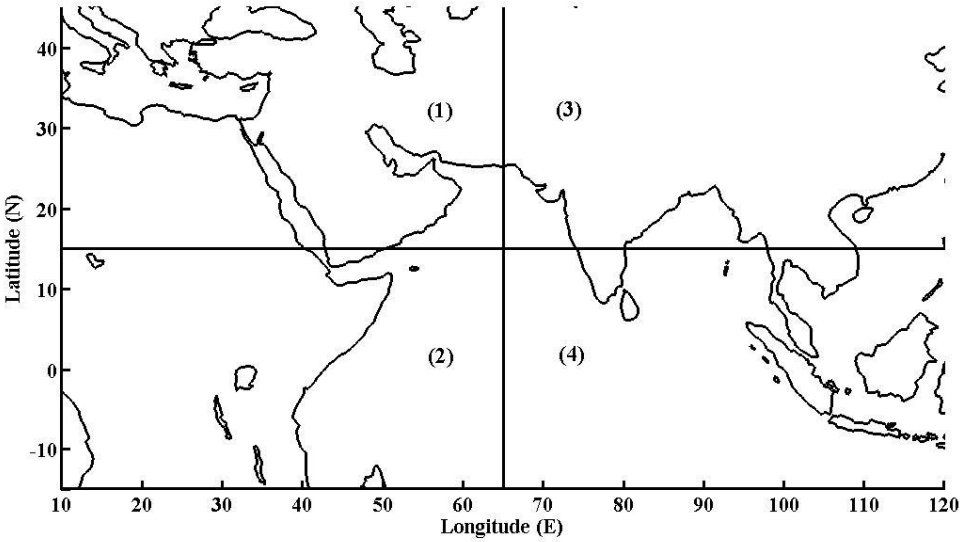

Figure 4. Regions representing the various aerosol sources for a point over the Arabian Sea. 1) Arabian Peninsula and North Africa, 2) Central Africa, 3) Indian sub-continent and 4) Indian Ocean and Southeast Asia.

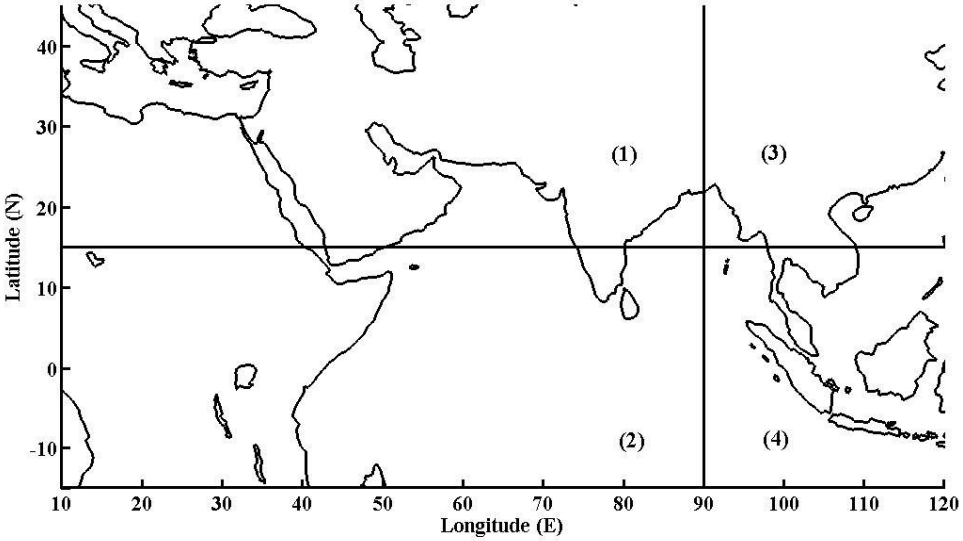

811

812 **Figure 5.** Regions representing the various aerosol sources for a point over the Bay of Bengal. 1)

813 India/Arabian Peninsula, 2) Indian Ocean, 3) North/Northeast India and East Asia and 4)

814 Southeast Asia.

815

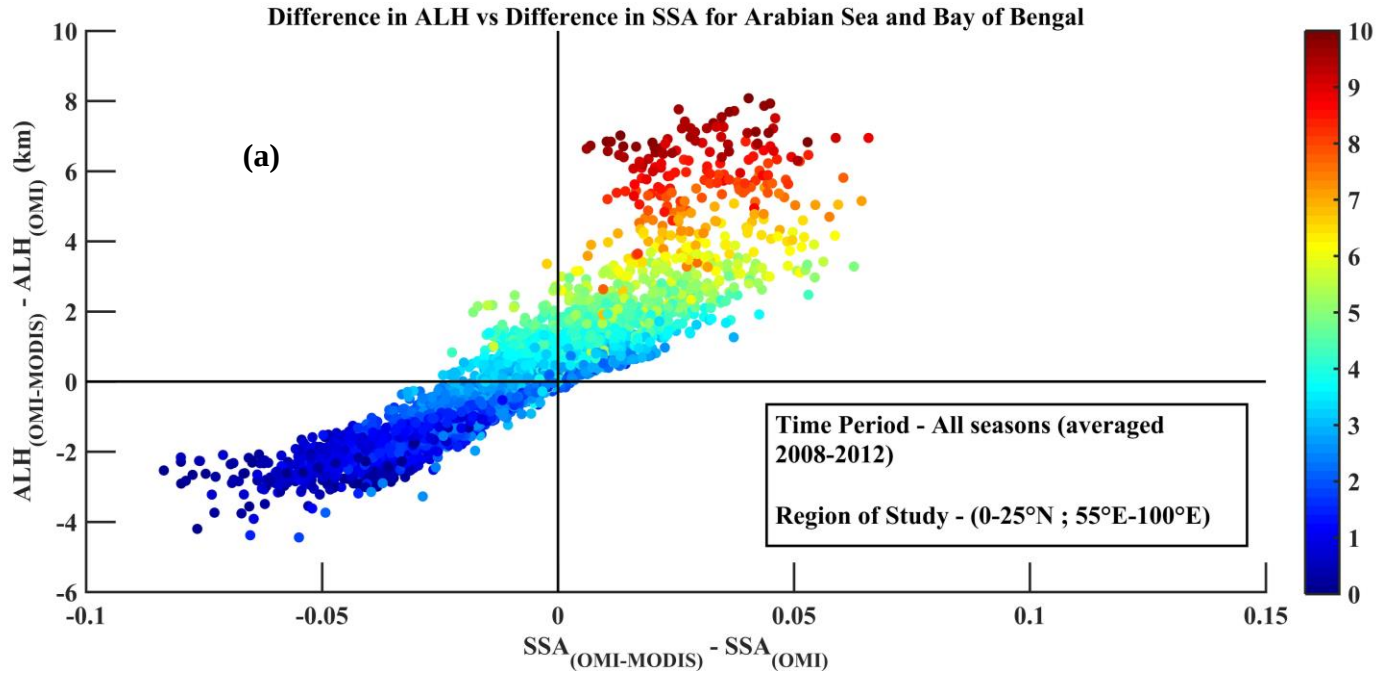

816

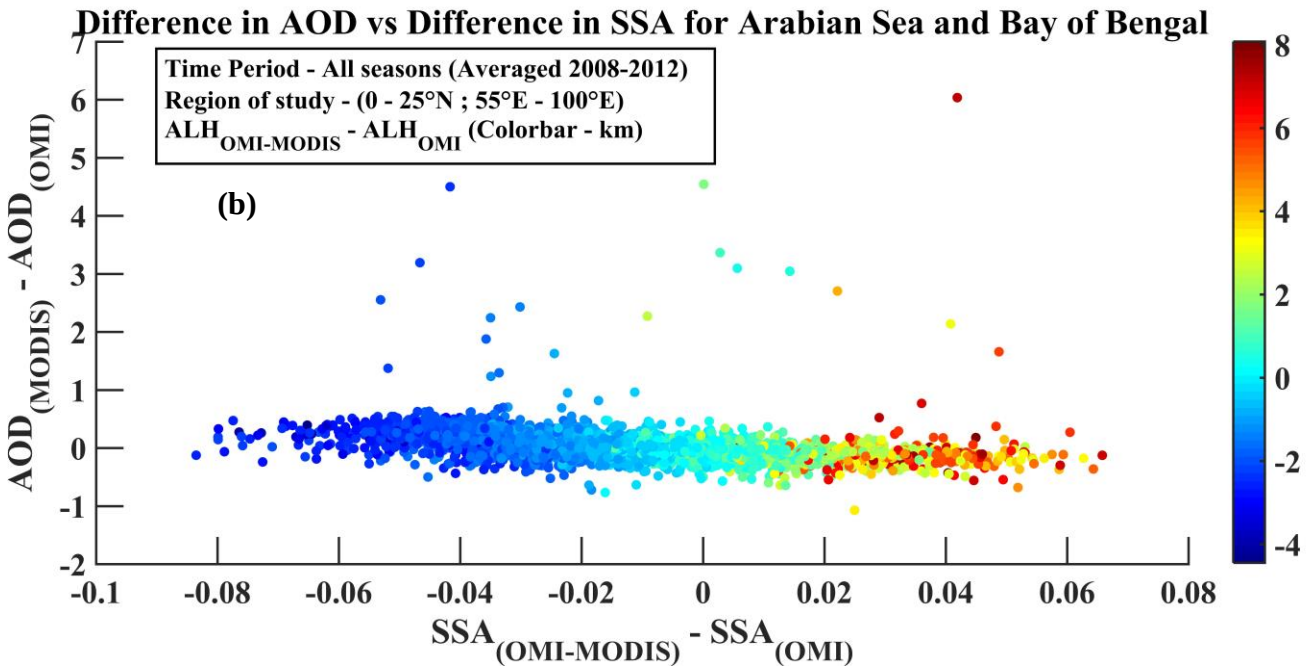

817

818 **Figure 6.** a) Difference in aerosol layer height (ALH - km) between OMI-MODIS and OMI vs.
819 difference in SSA over Arabian Sea and Bay of Bengal. The colorbar represents ALH estimated
820 by OMI-MODIS algorithm (km). At lower height (dark blue circles) estimated by OMI-MODIS
821 OMI overestimated SSA when the ALH was overestimated and vice versa at higher heights
822 estimated by OMI-MODIS b) Difference in AOD ($AOD_{MODIS} – AOD_{OMI}$) has been plotted with
823 difference in SSA ($SSA_{OMI-MODIS} – SSA_{OMI}$). An inverse relationship was observed. The colorbar
824 represents the difference in aerosol layer height (ALH - km) between OMI-MODIS and OMI.

825

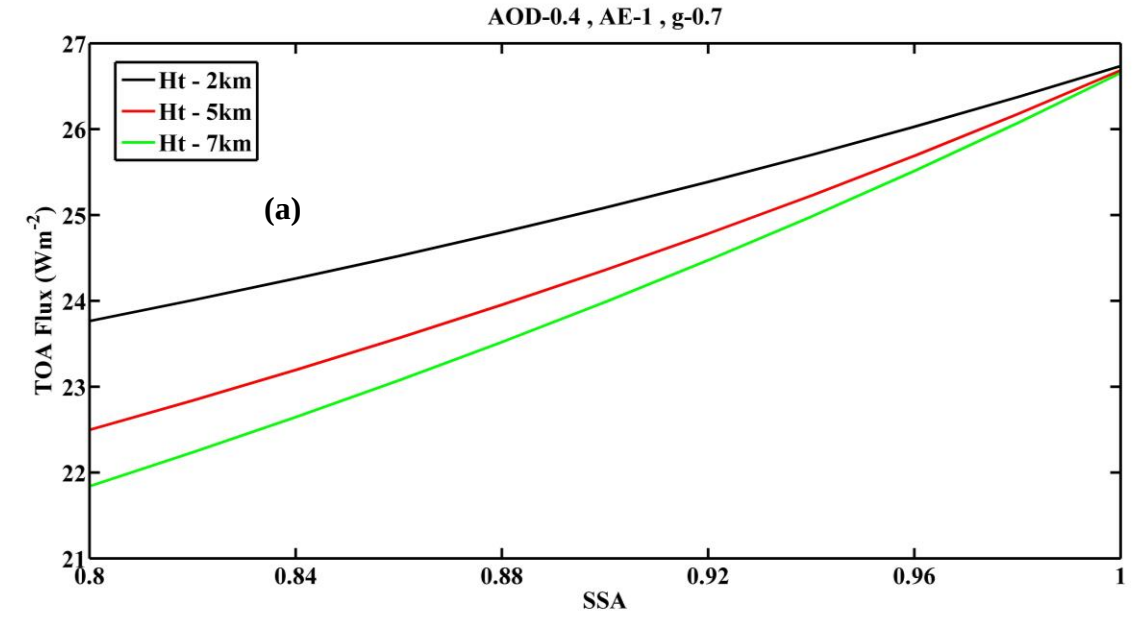

826

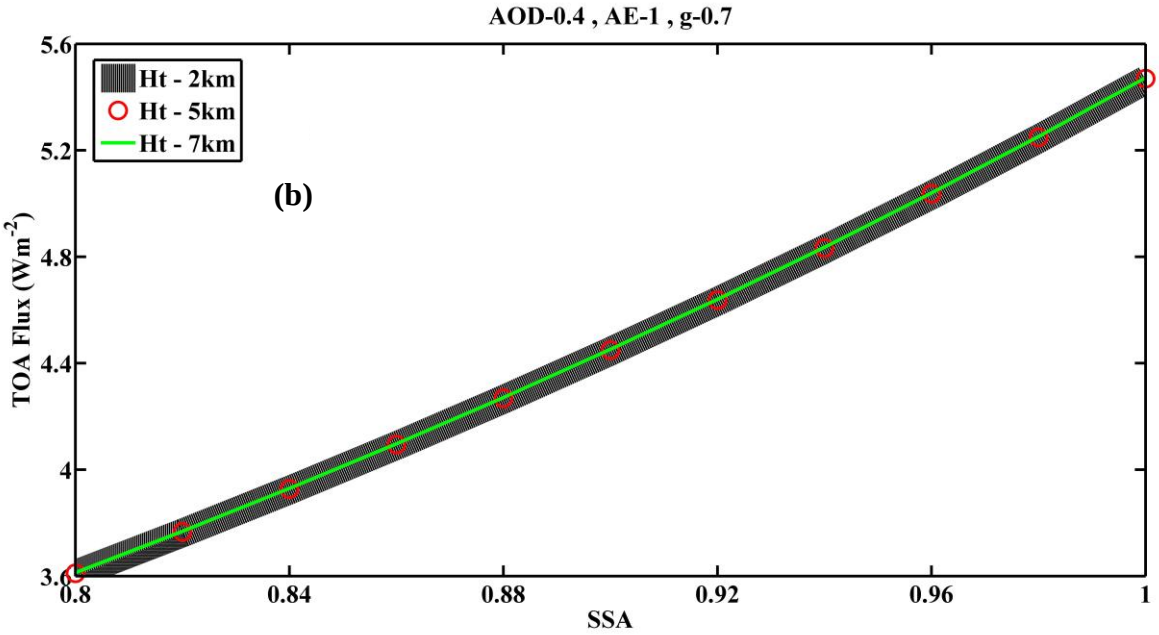

827

828 **Figure 7.** TOA flux calculated from SBDART for different SSA and ALH a) with Rayleigh

829 scattering and b) without Rayleigh scattering for UV (300-400nm)

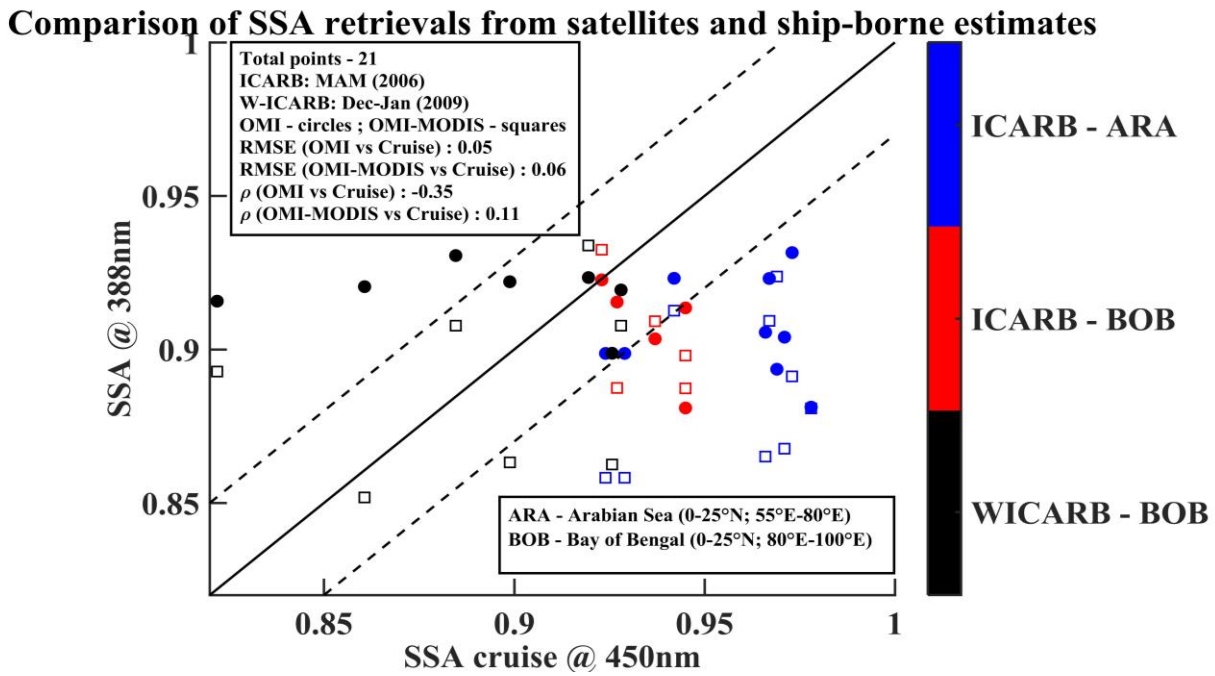

Figure 10. Comparison of SSA_{OMI} (circles), $SSA_{OMI\text{-}MODIS}$ (squares) with cruise measurements. Each point represents the mean SSA in a 2° box surrounding each cruise location averaged over the respective cruise time period. Due to the sparse nature of OMI-MODIS retrieval, the total number of points common to both the cruise and satellite estimates is only 21. The solid black line is the y=x line. The dotted lines represent ±0.03 range. The colorbar represents the cruise name and the region where the measurements are taken. ICARB (Integrated Campaign for Aerosols, Gases and Radiation Budget) during March-April-May (MAM) 2006 season; W-ICARB (Winter ICARB) during December-January (2008-2009); ARA (Arabian Sea); BOB (Bay of Bengal). Discrepancies between the satellite retrievals and cruise measurements were seen during the ICARB cruise when elevated aerosols were predominantly present over both the regions which might not be detected by the cruise measurements.

References	Method	Technique	Limitation

Herman et al., 1975; King, 1979; Eck et al., 1998; Dubovik and King, 2000; Torres et al., 2005	Ground-based observations	Inverse methods measurements of solar radiances and/or aerosol properties along with radiative transfer calculations	Measurements are spatially and temporally constrained
Dubovik et al., 2002	Global network – Aerosols Robotic Network (AERONET)	Inverse technique using near-real time measured direct and diffuse radiation	Only land-based, low coverage over remote oceanic regions
Kaufman, 1987; Zhu et al., 2011; Wells et al., 2012	Critical surface reflectance - where the net role of aerosol absorption and scattering becomes independent of aerosol optical thickness and is affected only by SSA	Over varying surface reflectance, the radiance difference between clear and hazy skies is measured using satellite images	Limited spatial variability of surface reflectance. Works only for few cases where there are large amount absorbing aerosols present

Kaufman et al., 2002b	Retrieve SSA in visible wavelengths	Sun-glint is used as a bright background to differentiate role of scattering from aerosol absorption	Only limited scenarios present and does not work on land when absorbing aerosols are present (Torres et al., 2005).
Diner et al., 1998; Remer et al., 2005	Multi Angle Imaging Spectroradiometer (MISR) and Moderate Resolution Imaging Spectroradiometer (MODIS)	Retrieves AOD and SSA in the visible and infrared region of solar spectrum	Surface reflectance influences the retrievals
Herman et al., 1997; Torres et al., 1998	Total Ozone Mapping Spectrometer (TOMS)	Aerosol index parameter is highly sensitive to the Rayleigh scattering thus acting as a bright background in the UV regime	Large pixel size prone to cloud contamination
Torres et al., 2002	Ozone Monitoring Instrument (OMI)	Similar technique as TOMS. Pre-defined aerosol models used.	Sensitive to aerosol layer height and still prone to cloud contamination

842

843 **Table 1.** Ground-based and Satellite-based indirect methods to retrieve SSA

844

845

Seasons \ Regions		1	2	3	4
DJF	500m	**57%**	0%	38%	5%
	1500m	**62%**	10%	19%	9%
	2500m	**81%**	14%	0%	5%
MAM	500m	19%	**43%**	19%	19%
	1500m	29%	**29%**	23%	19%
	2500m	**57%**	14%	24%	5%
JJA	500m	0%	24%	0%	**76%**
	1500m	19%	**67%**	0%	14%
	2500m	**62%**	33%	5%	0%
SON	500m	5%	24%	**47%**	24%
	1500m	14%	19%	**48%**	19%
	2500m	**38%**	10%	19%	33%

846

847 **Table 2.** Influence of various aerosol sources over Arabian Sea given as percentage of
848 trajectories originating from each source respectively. The maximum influence is given in black
849 bold. The different source regions are explained in text and Fig. 4.

Seasons \ Regions		1	2	3	4
DJF	500m	**72%**	0%	14%	14%
	1500m	**48%**	14%	10%	28%
	2500m	29%	33%	0%	**38%**
MAM	500m	19%	**48%**	0%	33%
	1500m	**57%**	29%	20%	14%
	2500m	**71%**	24%	0%	5%
JJA	500m	0%	**100%**	0%	0%
	1500m	5%	**95%**	0%	0%
	2500m	14%	**81%**	0%	5%
SON	500m	5%	**52%**	33%	10%
	1500m	5%	**43%**	**43%**	9%
	2500m	5%	**33%**	29%	**33%**

Table 3. Influence of various aerosol sources over Bay of Bengal given as percentage of trajectories originating from each source respectively. The maximum influence is given in black bold. The different source regions are explained in text and Fig. 5.